truded aluminum sheet. The panel and shroud fin design and location of temperature gages is shown in Fig. 2. Longitudinal fairing strips were used to protect the wires leading from the fin temperature gages to the telemetry section in the payload. Fin temperature gage no. 1 was mounted on a fin panel surface; no. 2 was recessed, being mounted in a region where bending loads were not critical.

Results

The results of the fin temperature tests are shown in Fig. 3. Fin temperature gage no. 1 ceased sensing temperature at approximately 19½ sec after launch, presumably being stripped off the surface by the windstream. A comparison between predicted and actual temperatures to that time shows reasonably close agreement. Temperature gage no. 2 continued to sense temperature in excess of 50 sec with reasonable agreement except for approximately 7 or 8 sec immediately after second-stage burnout.

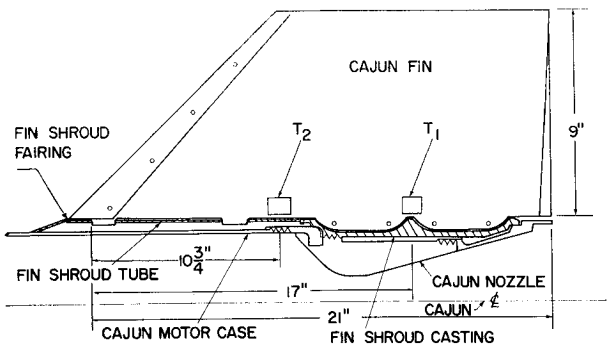

Fig. 2 Panel and shroud fin design; location of temperature gages.

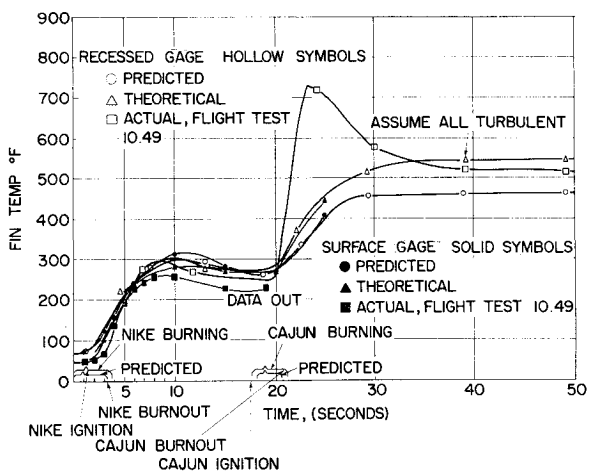

Fig. 3 Results of fin temperature tests.

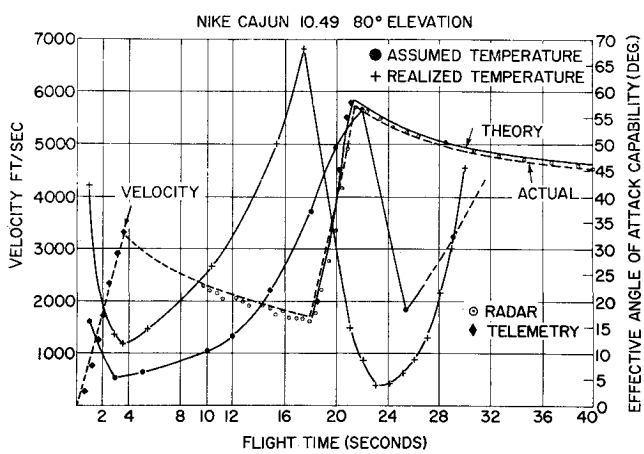

Fig. 4 Angle-of-attack capability.

Since wind gusts, stage separation, or thrust misalignment can cause disturbances in the flight path resulting in the rocket flying at some angle of attack until the disturbing force is overcome, calculations were made to determine the angle of attack capability based on the realized temperature. These calculations are compared with those based on design assumptions in Fig. 4. Two critical periods occur, at Nike burnout and at Cajun burnout. At both critical periods the fins can withstand loads approximating 4° angle of attack. In flight, the fin temperature appears to undergo a momentary surge at second-stage burnout which may be attributable either to 1) transient effect of stagnation temperature prior to heat conduction into the fin mass proper, or 2) heat conduction from the nozzle rather than from aerodynamic heating.

References

[1] Mamone, R. B., "Structural analysis of an advanced design Cajun-fin-shroud assembly," Space Vehicles Group Atlantic Research Corp. Preliminary Engineering Rept. 501-1B.

[2] Hansen, W. H. and Fischbach, F. E., "The Nike-Cajun sounding rocket," Engineering Research Institute, Univ. of Mich., Ann Arbor, Mich., Final Rept. 2453-1-F (March, 1957).

[3] Newell, H. E., Jr., *Sounding Rockets* (McGraw-Hill Book Co., Inc., New York, 1959), pp. 200–201.

Some Measurements of the Effects of Ring Baffles in Cylindrical Tanks

H. Norman Abramson* and Luis R. Garza†
Southwest Research Institute, San Antonio, Texas

RELATIVELY large lateral forces can be developed by liquid sloshing in the propellant tanks of large rocket boosters. Liquid resonant frequencies, if uncontrolled, could also give dynamic coupling with structural components and with the rocket's control system. For a given tank, the first-mode liquid resonant frequency can be substantially altered and its motion damped by means of either tank compartmentation or ring baffling of various types.

The present paper compares the effects of several types of ring baffles in a partially filled cylindrical tank undergoing forced vibration. Experimental resonant frequencies and damping values are obtained in a cylindrical tank at various depths below the liquid-free surface. This study may be regarded as an extension of the preliminary data given in Ref. 1, with particular emphasis on the effects of perforations in flat ring baffles. The equipment and procedures used are similar to those in Ref. 2. A 1.2-ft-diam rigid-wall cylindrical tank is supported by four dynamometers. The ring baffles were 0.018 to 0.030 in. thick, with width-to-radius ratio fixed at $W/R = 0.157$‡, and with varying degrees of perforation. All types were tested at three amplitudes of translation excitation and several baffle depths.

Liquid Resonant Frequencies

Figure 1 shows the first-mode liquid natural frequencies in terms of the dimensionless frequency parameter $2\omega^2 R/a$

Received April 17, 1964; revision received June 15, 1964. The results presented in this note were obtained during the course of research sponsored by NASA Marshall Space Flight Center under Contract No. NAS8-1555.

* Director, Department of Mechanical Sciences. Associate Fellow Member AIAA.

† Research Engineer, Department of Mechanical Sciences.

‡ The effects of baffle width are rather well delineated in Ref. 1.

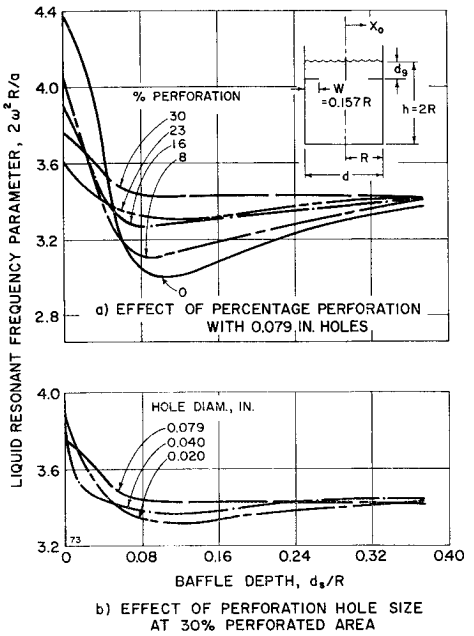

Fig. 1 Liquid resonant frequencies as functions of baffle depth.

(where a is the axial acceleration field on the tank and ω is the excitation frequency in rad/sec), vs the ring baffle depth d_s/R for various single ring baffles, where the over-all liquid depth is held fixed at $h/R = 2$. For single ring baffles having a width-to-radius ratio of $W/R = 0.157$, the liquid resonant frequency exhibits a maximum for $d_s/R = 0$ and decreases to a minimum near $d_s/R = 0.10$. For $d_s/R > 0.10$, frequencies increase with d_s/R and gradually approach the first liquid resonant frequency for a bare-wall cylindrical tank. For perforated baffles with 0.079-in.-diam holes at $d_s/R > 0.06$, the frequency increases as the perforated area is increased; for a given percentage perforated area, the frequency increases with hole size. Because of the rather significant effects of excitation amplitude, measurements were made for various values in the range $0.00184 \leqslant X_0/d \leqslant 0.00823$, and then all data were presented in terms of rms values.

Liquid Damping

The initial phase of this investigation was directed toward comparing experimental values of the damping ratio γ_s, obtained by the half-band width procedure from the resonance peaks of the experimental force response curves, with the theoretical values of γ_s calculated from Mile's equation[3] using liquid surface amplitudes, ζ_w, measured at the tank wall. Figure 2 compares experimental and theoretical damping for a solid ring baffle of $W/R = 0.157$; agreement is good, except for the region $0 < d_s/R < 0.125$, in which the experimental values are considerably greater than those predicted. The free-liquid surface in this region of d_s/R is quite complex and far from the smooth shape assumed in the theory.

Figure 3a shows damping ratios for percentage perforations from 8 to 30% with 0.079-in. holes; results for a solid ring and for a perforated ring having 23% area removed with 0.020-in. holes are included for comparison. At small d_s/R, the damping increases abruptly with percentage perforations less than 16%. Note that 23% perforated area with 0.020-in. holes gives the same damping as 8% perforated area with 0.079-in. holes.

Figure 3b shows the damping ratios for 30% perforated single ring baffles with hole sizes of 0.020, 0.040, and 0.079 in. The damping produced is consistently lower than that produced by the solid ring, but effectiveness improves as the hole size is decreased.

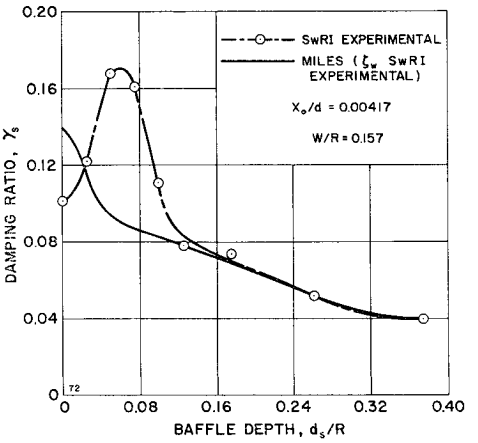

Fig. 2 Comparison of theory and experiment for damping provided by a flat solid ring baffle as a function of baffle depth.

Multiple ring baffles can be used to provide a high degree of damping for all liquid levels. The damping to be provided by such a system is controlled by proper spacing of the baffles. Tests were conducted with a set of two baffles, one above and the other below the liquid surface. The data indicate that, for an excitation amplitude of $X_0/d = 0.00417$, the baffle above the liquid is effective only at distances less than $0.125R$, and that the submerged baffle is effective from $d_s/R = 0$ to 0.375. Thus, to maintain some minimum acceptable damping γ_{min} for a series of ring baffles, the spacing should be the depth of the submerged baffle corresponding to γ_{min} from these tests plus the additional $d_s/R = 0.125$ for which the upper baffle is still effective.

Conclusions

A series of ring baffles can be used efficiently to damp liquid motion throughout the depth of a cylindrical tank. Perforated material having relatively small holes can be used effectively, reducing the ring baffle area by as much as 23% with no appreciable loss in damping effectiveness. Such

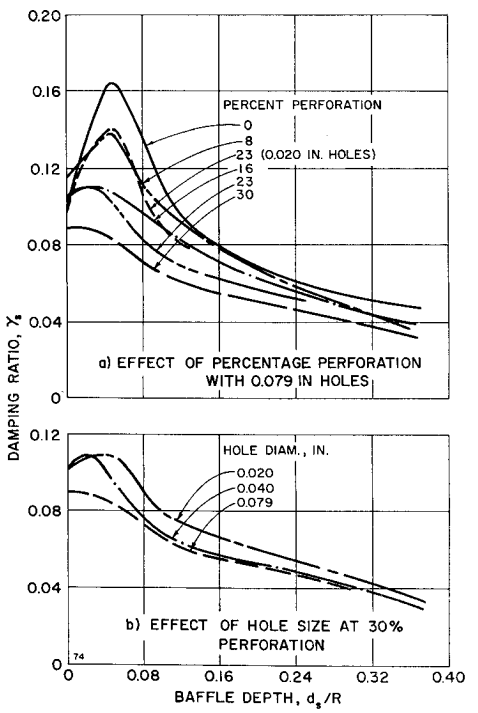

Fig. 3 Damping effectiveness as a function of baffle depth.

reduction in baffle area may be effectively used for additional baffles, thus increasing the minimum damping ratio value with no appreciable increase in baffle weight. The liquid natural frequencies are somewhat dependent on both the ring width and the ring baffle spacing. The first liquid resonant frequency increases over that of a bare wall tank only for baffle positions in the immediate vicinity of the liquid surface, and decreases below that of a bare wall tank for more deeply submerged ring baffles.

For a vehicle in which the first liquid resonant frequency is not critically coupled with the control system, ring baffle damping is therefore probably the most efficient means of introducing liquid damping into the propellant tanks. If, however, the liquid resonant frequencies are critical and must be shifted by rather significant amounts, other baffle systems should be considered.

References

[1] Silveira, M. A., Stephens, D. G., and Leonard, H. W., "An experimental investigation of the damping of liquid oscillations in cylindrical tanks with various baffles," NASA TN D-715 (May 1961).

[2] Abramson, H. N. and Ransleben, G. E., Jr., "Simulation of fuel sloshing characteristics in missile tanks by use of small models," ARS J. **30**, 603–612 (1960).

[3] Miles, J. W., "Ring damping of free surface oscillations in a circular tank," J. Appl. Mech. **25**, 274–276 (June 1958).

Gyroscopic Attitude Stabilization

RONALD L. HUSTON*
University of Cincinnati, Cincinnati, Ohio

Introduction

IN an earlier investigation,[1] the feasibility of gyroscopic attitude stabilization of satellites and space vehicles was examined and found to be realizable. The stabilization was attained through an internally moving disk gyro, but gravitational effects were neglected. Thomson[2] has studied stabilization, including gravitational effects, but required the spinning of the entire satellite. Kane and Sobala,[3] also including gravitational effects, have demonstrated the practicability of obtaining stabilization through internally moving particles. The purpose of the present investigation is to explore further, by including gravitational effects, the concept of stabilization through an internally moving disk gyro.

Governing Equations

The system to be studied is shown in Fig. 1 where V represents a rotationally symmetric satellite with L_3 being the axis of symmetry. D represents a circular disk gyro whose axis is L_3 and whose mass center C coincides with the mass center of V. L_1 and L_2 are axes in the plane of D, which form with L_3 a dextral set. Because of the symmetry, these axes are centroidal principal inertia axes, although L_1 and L_2 are not fixed in either V or D. Finally, parallel to each axis, there is a unit vector $\mathbf{n}_i$ $(i = 1, 2, 3)$.

The system is considered to be in a motion in which C describes a circular orbit. Let $\dot{\theta}$ represent the angular rate of change, in inertial space, of a radial line drawn from O, the orbit center, to C. By considering a configuration in which L_3 is normal to the orbit plane and L_1 is parallel to OC in the direction OC, three angles, α, β, and γ, may be introduced and defined by successive dextral rotations about the axes

Received June 8, 1964.

* Assistant Professor of Mechanics.

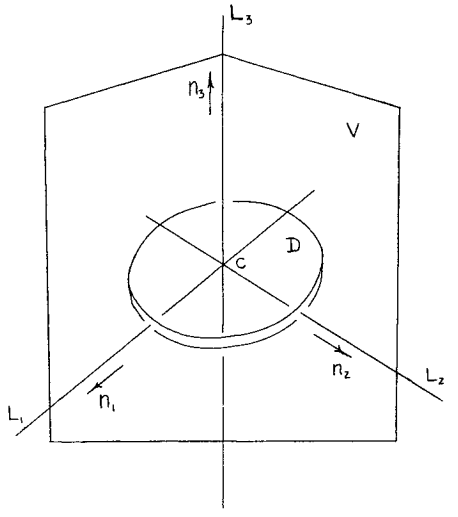

Fig. 1 Satellite with disk gyro.

L_1, L_2, and L_3. The angular velocity of V in inertial space, in which the orbit is taken to be fixed, is then given by

$$\boldsymbol{\omega}_V = (\dot{\alpha}\cos\beta - \dot{\theta}\sin\beta\cos\alpha)\mathbf{n}_1 + (\dot{\theta}\sin\alpha + \dot{\beta})\mathbf{n}_2 + (\dot{\gamma} + \dot{\alpha}\sin\beta + \dot{\theta}\cos\alpha\cos\beta)\mathbf{n}_3 \quad (1)$$

Regarding D as having an angular speed Ω with respect to V, the corresponding angular velocity of D is

$$\boldsymbol{\omega}_D = \boldsymbol{\omega}_V + \Omega\mathbf{n}_3 \quad (2)$$

The kinetic energy of the system is then

$$K = (\tfrac{1}{2})[mr^2\dot{\theta}^2 + I_1\omega_1^2 + I_2\omega_2^2 + (I_3 - 2I_D)\omega_3^2 + 2I_D(\Omega + \omega_3)^2] \quad (3)$$

where r is the orbit radius OC, m is the combined mass of V and D, I_i $(i = 1, 2, 3)$ are the combined moments of inertia of V and D with respect to C about the L_i axes, I_D is the moment of inertia of D with respect to C about the L_1 axis, and ω_i are the $\mathbf{n}_i$ measure numbers of $\boldsymbol{\omega}_V$, obtainable from Eq. (1).

The gravitational forces, which have been investigated by Nidey[4] and others, may be represented by a single force passing through C together wth a couple of torque $\mathbf{T}$ given by

$$\mathbf{T} = 3\dot{\theta}^2(I_1 - I_3)\sin\beta\cos\beta\mathbf{n}_2 \quad (4)$$

By considering α, β, and γ as generalized coordinates in the sense of Lagrangian mechanics, Eqs. (4) and (1) lead to the generalized forces

$$F_\alpha = F_\gamma = 0 \qquad F_\beta = 3\dot{\theta}^2(I_1 - I_3)\sin\beta\cos\beta \quad (5)$$

The governing equations of motion are then obtained through Eqs. (3) and (5) and are ot the form

$$(d/dt)(\partial K/\partial\dot{\alpha}) - \partial K/\partial\alpha = F_\alpha \quad (6)$$

If, for the purposes of stability considerations, α and β are considered small, these governing equations may be written

$$\ddot{\alpha} - c_1\dot{\beta} + c_2\alpha = 0 \quad (7)$$

$$\ddot{\beta} + c_1\dot{\alpha} - c_3\beta = 0 \quad (8)$$

$$(\dot{\theta} + \dot{\gamma})I_3 + 2I_D\Omega = \text{const} \quad (9)$$

where the coefficients c_1, c_2, and c_3 are given by

$$c_1 = [2 - (I_3/I_1)]\dot{\theta} - (I_3/I_1)\dot{\gamma} - 2\Omega(I_D/I_1) \quad (10)$$

$$c_2 = -(I_3/I_1)\dot{\gamma}\dot{\theta} + [1 - (I_3/I_1)]\dot{\theta}^2 - 2\Omega\dot{\theta}(I_D/I_1) \quad (11)$$

$$c_3 = -(I_3/I_1)\dot{\gamma}\dot{\theta} + 4[1 - (I_3/I_1)]\dot{\theta} - 2\Omega\dot{\theta}(I_D/I_1) \quad (12)$$